Environmental Science: Atmospheres

ROYAL SOCIETY OF CHEMISTRY

PAPER

View Article Online
View Journal | View Issue

Cite this: *Environ. Sci.: Atmos.*, 2025, **5**, 1158

Airborne cloud water pH measurements in diverse regions: statistics and relationships with constituents

Kayla M. Preisler, [a] Ewan C. Crosbie,[bc] Miguel Ricardo A. Hilario,†[a] Grace Betito,[a] Rachel A. Braun,[d] Andrea F. Corral, [e] Eva-Lou Edwards,[b] Alexander B. MacDonald,[f] Ali Hossein Mardi, [g] Michael A. Shook, [b] Connor Stahl,[e] Edward L. Winstead,[bc] Kira Zeider,‡[e] Luke D. Ziemba[b] and Armin Sorooshian *[ae]

Airborne cloud water measurements are examined in this study, with a focus on pH and interrelationships with influential species for three regions: the Northwest Atlantic (winter and summer 2020–2022), the West Pacific (summer 2019), and the Northeast Pacific (summers between 2011 and 2019). Northwest Atlantic results are categorized into three ways: data closer to the U.S. east coast for (i) winter, (ii) summer, and (iii) summertime measurements over Bermuda. The median pHs are as follows: Northwest Atlantic winter/summer = 4.83/4.96, Bermuda = 4.74, West Pacific = 5.17, and Northeast Pacific = 4.40. The regions exhibit median pH values of ~4–6 across various altitude bins reaching as high as 6.8 km, with the overall minimum and maximum values being 2.92 and 7.58, respectively (both for the Northeast Pacific). Principal component analysis of species to predict pH shows that the most influential principal component is anthropogenic in nature. Machine leaning modeling suggests that the most effective combination of species to predict pH includes some subset of oxalate, non-sea salt Ca^{2+}, NO_3^-, non-sea salt SO_4^{2-}, and methanesulfonate. These results demonstrate that cloud water acidity is relatively well constrained between a pH of 4 and 5.5 and that anthropogenic activities impact regional cloud water pH in the areas examined, with dust offsetting acidity at times.

Received 19th June 2025
Accepted 26th August 2025

DOI: 10.1039/d5ea00070j

rsc.li/esatmospheres

Environmental significance

Cloud water acidity has significant implications for atmospheric chemistry and effects on human health and ecosystems due to its deposition in the form of precipitation. Cloud water acidity, as represented by pH, can also provide clues about air mass sources influencing an area. It is challenging to characterize the pH of clouds over the ocean, and to fill that gap, this study used aircraft to collect such data over the Northwest Atlantic, the West Pacific, and the Northeast Pacific. Each region shows distinct relationships between the chemical constituents and pH levels. Results indicate a strong influence of anthropogenic emissions, with occasional influence due to dust, on cloud water pH in each region, which is generally constrained between 4 and 5.5. This research supports the improvement of air quality management and encourages future research on cloud water pH in other regions, especially due to the growing interest in aerosol–cloud interactions.

1 Introduction

Cloud water acidity has important implications for the phase partitioning of semi-volatile gases, aqueous-phase chemical reactions, pollutant lifetimes, and effects on health and ecosystems after deposition. pH is the measurement of acidity and is influenced by the chemical constituents in cloud water. By studying the acidity and chemical composition of water droplets, insights can be gained about air mass sources impacting clouds and their effects on wet deposition.[1,2] Cloud water acidity can provide insights into aerosol–cloud interactions, which represent the largest source of uncertainty in estimates of anthropogenic radiative forcing.[3,4] These interactions involve aerosol effects on clouds (*e.g.*, droplet activation)

[a]*Department of Hydrology and Atmospheric Sciences, University of Arizona, Tucson, AZ, 85721, USA. E-mail: armin@arizona.edu*
[b]*NASA Langley Research Center, Hampton, VA, 23681, USA*
[c]*Analytical Mechanics Associates, Inc., Hampton, VA, 23666, USA*
[d]*School of Sustainable Engineering and the Built Environment, Arizona State University, Tempe, AZ, 85287, USA*
[e]*Department of Chemical and Environmental Engineering, University of Arizona, Tucson, AZ, 85721, USA*
[f]*Department of Environmental Sciences, University of California, Riverside, Riverside, CA, 92521, USA*
[g]*Department of Civil and Environmental Engineering, Virginia Tech, Blacksburg, VA 24061, USA*
† Now at Space Science and Engineering Center, University of Wisconsin-Madison, Madison, WI, 53706, USA.
‡ Now at Office of Land & Emergency Management, EPA (through Oak Ridge Institute of Science and Education), Washington, D.C., 20004, USA.

and cloud effects on aerosol, such as aqueous chemistry[5] and wet scavenging to remove aerosol from clouds.[6,7] The subset of aerosol particles that act as cloud condensation nuclei (CCN) can directly impact cloud water pH.[8,9] In contrast, after wet scavenging and precipitation, any particles remaining in the air after droplet evaporation that did not deposit to the surface could have altered properties relative to the original CCN.

Studies examining cloud water pH in various regions (Table 1) provide contextual information for this work. Shah *et al.* (2020)[10] compiled global cloud water data to investigate pH measurements for comparison with the GEOS-Chem model and concluded that the observed global mean cloud water pH is 5.2 ± 0.9, with a range from 3 to 8. The lowest pH values were observed over East Asia, dropping below 4.3 in China and Japan. pH values were low over the North Pacific, averaging around 4.5. In the U.S., the average pH ranges from 4 to 5, similar to the pH in Europe.[10] Gioda *et al.* (2011)[11] collected cloud water samples on a mountaintop in Puerto Rico 300 m above cloud base and found an average pH of 5.8. This is a typical average pH for a remote site with little influence from anthropogenic emissions.[11] This is comparable to the Sinhaged Hill Station in India, with a reported average pH value of 6.0, ranging from 4.7 to 7.4.[12] This remote site is covered with vegetation but is influenced by wood-burning emissions from cooking.[12] A study by Sun *et al.* (2010)[13] on Mt. Heng, China, found an average cloud water pH of 3.80, ranging from 2.91 to 6.91. On Mt. Tai Mo Shan, Hong Kong, Li *et al.* (2020)[14] reported a comparable average pH of 3.63 and a range from 2.96 to 5.94. Anthropogenic

Table 1 Relevant information from previous work, sorted chronologically by the study period, documenting cloud water pH over different regions. The table is also divided by cloud water samples collected by aircraft and *via* surface measurements on mountaintops

Location	Study period	Sample #	Average	Median	Range	Reference
Cloud water samples collected by aircraft						
Hawaii	Jun 1980	5	4.46	4.5	4.2–4.7	Parungo *et al.*, (1982)[15]
Northwestern Pacific Ocean and Japan Sea	Dec 1996–Feb 1997	6	—	—	3.8–5.0	Watanabe *et al.*, (2001)[16]
Pacific Ocean	Jul 2001	50	—	4.01	3.26–4.82	Straub *et al.*, (2007)[17]
Northern Michigan	Jun–Aug 2005	20	4.4	—	2.2–5.2	Hill *et al.*, (2007)[18]
Southeastern Pacific Ocean	Oct–Nov 2008	72	4.3	—	2.9–7.2	Benedict *et al.*, (2012)[19]
Northeastern Pacific Ocean	Jul–Aug 2011	82	4.46	—	2.92–7.58	Wang *et al.*, (2014)[20]
Northeastern Pacific Ocean	Jul–Aug 2011, 2013, 2015	235	4.26 (coupled clouds) and 4.48 (decoupled clouds)	—	—	Wang *et al.*, (2016)[1]
Northeastern Pacific Ocean	Jul–Aug 2013	48	4.3	—	—	Prabhakar *et al.*, (2014)[21]
Metro Manila, Philippines	Aug–Oct 2019	159	5.04	5.19	3.79–5.93	Stahl *et al.*, (2021)[22]
Cloud water samples collected on mountaintops						
Alaska	Aug–Sep 1984, Jul–Aug 1985	20	4.49	4.80	—	Bormann *et al.*, (1989)[23]
Mary's Peak, Oregon	Jun–Nov 1985	14	4.67	5.21	—	
Mt. Washington, New Hampshire	Jun–Aug 1984–2010	—	4.3	—	—	G. L. D. Murray *et al.*, (2013)[24]
Mt. Mitchell, North Carolina	May–Jun 1986–1987	6 4	3.45 (continental) 3.29 (marine)	— —	3.09–4.17 2.99–3.83	Deininger and Saxena *et al.*, (1997)[25]
Cheeka Peak Observatory, Washington State	May 1993	102	4.2	—	—	Vong *et al.*, (1997)[26]
Whiteface mountain, New York	1994–2021	9429	—	3.78 (1994) 5.34 (2021)	2.44–7.08	Lawrence *et al.* (2023)[27]
Puy de Dôme, France	2001–2011	143	5.5	5.6	3.1–7.6	Deguillaume *et al.*, (2014)[28]
East Peak Puerto Rico	Dec 2004–Mar 2007	45	5.8	—	—	Gioda *et al.*, (2011)[11]
Mt. Elders, Arizona	Jun–Sep 2005–2007	—	—	6.64	5.12–6.66	Hutchings *et al.*, (2009)[29]
Sinhagad hill station southwest of Pune, India	June 2007–Dec 2010	123	6.0	—	4.7–7.4	Budhavant *et al.*, (2014)[12]
Mt. Tai, China	2007–2008	243	4.60	4.34	2.56–7.64	Guo *et al.*, (2012)[30]
Mt. Heng, China	Mar–May 2009	38	3.80	—	2.91–6.91	Sun *et al.*, (2010)[13]
Mt. Schmücke, Germany	Sep–Oct 2010	60	4.29	4.56	3.6–5.3	van Pinxteren *et al.*, (2016)[31]
Mt. Lu, China	Aug–Sep, 2011–2012	141	3.79	—	2.75–5.84	Sun *et al.*, (2015)[32]
Mt. Tai, China	Jul–Oct 2014	85	5.87	—	3.80–6.93	J. Li *et al.*, (2017)[33]
Mt. Tai, China	Jun–Aug 2015	10	4.9	—	3.6–6.6	Zhu *et al.*, (2018)[34]
Mt. Tai Mo Shan, Hong Kong	Oct–Nov 2016	32	3.63	—	2.96–5.94	Li *et al.*, (2020)[14]

emissions influence both Mt. Heng and Mt. Tai, with the former being heavily influenced by acid deposition due to its proximity to China's leading industrial regions.[13]

Airborne cloud water research provides insights into marine environments and their cloud properties. For example, airborne measurements collected over the southeast Pacific Ocean (VOCALS-Rex) revealed an average pH of 4.3 and a range from 2.9 to 7.2.[19] Airborne measurements over the northeastern Pacific Ocean (E-PEACE) showed a comparable average (4.46) and range (2.92–7.58) to the southeastern Pacific Ocean.[20] The wide range of pH for the maritime clouds in VOCALS-Rex and E-PEACE is surprising, considering other studies on maritime clouds found a narrower range. For example, Straub *et al.* (2007)[17] and Watanabe *et al.* (2001)[16] observed a pH range of 3 to 5 for maritime clouds (Table 1).

The chemical composition of CCN and trace gases impacting cloud water differs between regions, leading to distinct interrelationships with pH. Lower pH values can indicate anthropogenic emissions (sulfur dioxide, nitrogen oxides, and organic acids), while higher pH values can indicate alkaline substances (ammonia and non-volatile cations).[2,35] For example, Gioda *et al.* (2011)[11] observed that the pH decreased with air masses from anthropogenic influences of NO_3^- and SO_4^{2-}. Similarly, Benedict *et al.* (2012)[19] noted lower pH values and higher sulfur dioxide and sulfate concentrations near the shore in the southeastern Pacific Ocean. Wang *et al.* (2014)[20] observed the lowest pH values off the central coast of California when there were high levels of vanadium and nitrate, which were traced to ship emissions. Wang *et al.* (2016)[1] subsequently showed for the same region that cloud water pH is generally lower for clouds coupled to the ocean (4.26) as compared to decoupled clouds (4.48); this result was also recently demonstrated for the Northwest Atlantic by Zeider *et al.* (2025).[9] It is crucial to investigate the chemical composition of cloud water and cloud water acidity to improve air quality management and policy planning for health and ecosystems.

The present work examines airborne cloud data in three diverse marine regions: the Northwest (NW) Atlantic, the West (W) Pacific, and the Northeast (NE) Pacific. Despite many decades of research investigating cloud water acidity, there is less research on marine environments with data collected by aircraft. The campaigns in each region offer many samples (≥237 per region) of pH and constituents to characterize the acidity. In addition to regional comparisons, we examine the vertical characteristics, interrelationships between pH and other measured species, and seasonal differences as samples were collected in both summer and winter in one of the regions where the mission design focused on seasonal differences in aerosol–cloud interactions (Northwest Atlantic).

2 Data and methods

2.1 Field campaigns

2.1.1 Northwest Atlantic (ACTIVATE). The Northwest Atlantic dataset is associated with the NASA Aerosol Cloud meTeorology Interactions oVer the western ATlantic Experiment (ACTIVATE) airborne field campaign. The campaign focused on characterizing relationships between aerosol–cloud interactions, meteorology, and marine boundary layer clouds over the Northwest Atlantic during winter and summer for each year between 2020 and 2022.[36] The Northwest Atlantic dataset represents clouds ranging from stratiform to cumulus clouds. Two NASA Langley research aircraft flew in spatial coordination: the higher-flying King Air and the lower-flying HU-25 Falcon (hereafter called Falcon). The King Air flew steadily at ~9 km, releasing dropsondes and using remote sensing to retrieve particle and cloud properties below the aircraft. The Falcon generally remained at <3 km altitude and conducted *in situ* measurements of trace gases, aerosol particles, clouds, precipitation, and atmospheric state parameters within and just above the marine boundary layer. The data used in this paper will be exclusively from the Falcon, with 271 cloud water samples collected during the 174 research flights, most of which were based out of NASA Langley Research Center (LaRC). An intensive period of operations was based out of Bermuda in June 2022. Due to its significant spatial separation from the rest of the ACTIVATE flights, this subset of data (14 samples) is separated for parts of the analysis of this study. For the flights closer to the U.S. East Coast, results are also separated based on season: winter = 178 samples; summer = 79 samples. Fig. 1 shows spatial maps of pH for the Northwest Atlantic samples and the next two regions. Full details of ACTIVATE's flights and instruments can be found elsewhere.[37] Cloud water was collected using the Axial Cyclone Cloud-water Collector (AC3 (ref. 38)).

2.1.2 West Pacific (CAMP^{2}Ex). The West Pacific data stem from the NASA Cloud, Aerosol, and Monsoon Processes Philippines Experiment (CAMP^{2}Ex), which aimed to characterize

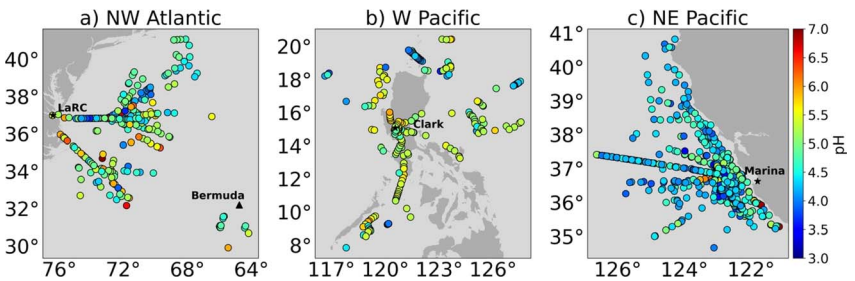

Fig. 1 Spatial maps of cloud water pH measured over the (a) Northwest Atlantic, (b) West Pacific, and (c) Northeast Pacific. Markers are colored by pH, and the air bases used are labeled on each map. LaRC refers to the NASA Langley Research Center in Hampton, Virginia.

aerosol processes, cloud physics, and radiation effects over Southeast Asia during the southeast monsoon.[39] The NASA P-3B Orion, Stratton Park Engineering Company (SPEC) Learjet 35, and various satellites, a ship, and other surface sensors were utilized for this campaign.[22,39] This work uses cloud water data from the NASA P-3B Orion aircraft collected at altitudes ranging from 0.2 to 6.8 km.[22,40] A total of 238 cloud water samples were collected during the 19 research flights from 23 August to 5 October 2019. Flights were flown out of the Clark International Airport in the Philippines. Cloud water was collected using the AC3 mentioned above[38] CAMP^{2}Ex samples were collected under conditions marked by tropical storm convective cores, cold pools, broken shallow cumulus clouds, and congestus clouds.

2.1.3 Northeast Pacific. Data used from the Northeast Pacific were derived from the following six campaigns sponsored by the Office of Naval Research: Eastern Pacific Emitted Aerosol Cloud Experiment (E-PEACE, 2011), Nucleation in California Experiment (NiCE, 2013), Biological and Oceanic Atmospheric Study (BOAS, 2015), Fog and Stratocumulus Evolution Experiment (FASE, 2016), MONterey Aerosol Research Campaign (MONARC, 2019), and Marine Aerosol Cloud And Wildfire Study (MACAWS, 2018). Flights were conducted with the Naval Postgraduate School Twin Otter based out of Marina, California, between May and August, with a complete description of the aircraft missions and instruments provided elsewhere.[41] A total of 517 cloud water samples were collected using a slotted-rod collector,[20,42] with the data representative of summertime stratocumulus clouds.

2.2 Cloud water collectors and chemical analysis

2.2.1 Axial Cyclone Cloud-water Collector (AC3). The cloud water data collected for the Northwest Atlantic and West Pacific relied on the Axial Cyclone Cloud-water Collector (AC3). The AC3 concept expands and revises the axial cyclone concept described by Straub and Collett (2004).[43] The AC3 samples cloud water by separating droplets from the primary airflow. The axial cyclone technique involves imparting swirl on an axial flow (using an in-line stator) and then collecting cloud water along the direction of the free stream. This creates a helical flow pattern resulting in centrifugal separation of large particles and droplets from the air stream. For optimal airborne cloud water collection, the cloud droplets are migrated to the outer walls for capture, while aerosol particles remain in the air stream to be exhausted. This design allows for a high volume of collected cloud water during cloud penetrations and the possibility of high temporal resolution sampling.[38]

Samples in the Northwest Atlantic and West Pacific were collected when the aircraft was in cloud, and a shutter was used to reduce contamination when the aircraft was out of cloud.[22,37] For the Northwest Atlantic, sample duration times ranged from 25 s to 83 min, while in the West Pacific, durations ranged between 15 s and 13 min. Longer duration samples usually are due to a combination of extended periods when the aircraft was out of cloud and/or very low liquid water content values in clouds. For both regions, the samples were collected under vacuum through a Teflon sampling line inside the respective aircraft platforms used and deposited in 15 mL high-density polyethylene centrifuge tubes. Samples were collected and stored in coolers with ice packs during flights to reduce decomposition. After flights, samples were kept refrigerated until analysis in a laboratory for pH and other chemical speciation analyses.[22,37] Flights from all of the regions in this study were done during the daytime, and thus it is not expected that differences in time of day for sample collection impacted the results.

2.2.2 Slotted-rod collector. Cloud water was collected over the Northeast Pacific using the Mohnen slotted-rod collector. The rod is based on the principle of inertial impaction of droplets onto a cylinder.[44] When droplets move with the air around the cylinder, larger ones will be intercepted by the cylinder due to their inertia.[45] When in a cloud, the slotted rod collector was manually extended out of the top of the Twin Otter aircraft, with liquid droplets deposited in high-density polyethylene bottles that were kept cool with ice packs and then refrigerated after flights until laboratory analysis was conducted.[46,47] Sample collection duration ranged from 2 to 90 min.

It is important to acknowledge that this study compared data collected from two separate cloud water collectors. However, the Mohnen slotted-rod collector was directly compared to the AC3 on the Naval Postgraduate School Twin Otter during the Fog and Stratocumulus Evolution (FASE), which is one of the campaigns used in this study.[38] The results found that the two collectors showed good agreement with the comparison of trace species concentrations. This does not preclude differences in sample collection due to usage of different aircraft; however, still the results within a fixed region intercomparing species concentrations to pH are robust owing to reliance on the same measurement setup. Further information about the comparison can be found in Crosbie *et al.* (2018).[38]

2.2.3 Laboratory analysis. Each cloud water sample was separated into fractions for different types of analysis: pH, water-soluble ionic composition (Ion Chromatography, IC), and water-soluble elemental composition (Inductively Coupled Plasma Mass Spectrometry, ICP-MS).[41] Table 2 details the instruments used in each region, the duration of sample collection, and the species list. IC analysis was conducted for all regions, but ICP-MS was done only for the Northwest Atlantic and Northeast Pacific. While samples were efficiently analyzed for pH and IC post-flight for most campaigns, ICP-MS analysis took place weeks later for all campaigns. There is the possibility of error in these measurements owing to sample storage even while being kept cool during and after flights.[2] Measurement uncertainties for the analytical techniques used are summarized in detail by numerous other studies using these field campaign datasets (Northwest Atlantic,[37] West Pacific,[39] and Northeast Pacific[41]), with uncertainties being species-dependent and typically <30%. The data quality control process included flushing of the cloud water collectors with ultrapure MilliQ water (18.2 MΩ cm) before and after flights, with blank samples collected prior to flights after cleaning. Blank concentrations were subtracted from true samples for individual species.

The anions included in this study are methanesulfonate (MSA), oxalate, NO_3^-, and the calculated NSS-SO_4^{2-}. The

Table 2 Summary of sample collection and laboratory analysis details for each region, including the number of cloud water samples collected and the cloud type for each region. Descriptions extending across multiple columns indicate that the same information applies to all regions covered by those column (*e.g.*, the same IC species were measured in all three regions)

	Northwest Atlantic	West Pacific	Northeast Pacific
# of cloud water samples	271	238	517
Altitude range	0.1–3.0 km	0.1–6.8 km	0.1–1.0 km
IC species	MSA, oxalate (C_2O_4), NO_3^-, Na^+, NH_4^+, NSS-K^+, NSS-Ca^{2+}, and NSS-SO_4^{2-}		
ICP-MS species	Al, V, Mn, Ni, Cu, Zn, As, Rb, Cd, and Pb	Not included	Al, V, Mn, Ni, Cu, Zn, As, Rb, Cd, Pb
Time resolution	25 s–83 min	15 s–13 min	2–90 min
pH meter and probe	Orion Star™ A211 pH meter paired with an Orion™ 8103BNUWP ROSS Ultra™ pH electrode; calibrated with pH 4.00 and 7.00 buffer solutions		Oakton model 110 pH meter that was calibrated with pH 4.01 and 7.00 buffer solutions (E-PEACE, NiCE, and BOAS) and a Thermo Scientific Orion 8103BNUWP ROSS Ultra Semi-Micro pH probe (FASE, MACAWS)
Ion Chromatography, IC	Dionex ICS-2100: Anions were measured using the Dionex IonPac AS11-HC 2 mm × 250 mm column, a Dionex AERS 500e suppressor, and potassium hydroxide as an eluent. Cations were measured using the Dionex IonPac CS12A 2 × 250 mm column, a Dionex CERS 500e suppressor, and MSA as an eluent		
Inductively Coupled Plasma Mass Spectrometry, ICP-MS	Agilent 7700 series	Not included	Agilent 7700 series for E-PEACE, NiCE, MONARC, and BOAS; Triple Quadrupole Inductively Coupled Plasma Mass Spectrometry (ICP-QQQ MS; Agilent 8800 series) for FASE and MACAWS
Cloud type	Stratiform to cumulus clouds	Tropical storm convective cores, cold pools, broken shallow cumulus clouds, and congestus clouds	Stratocumulus clouds

cations included in this study are Na^+ and NH_4^+, along with the calculated NSS-K^+ and NSS-Ca^{2+}. The ICP-MS species used in the Northwest Atlantic and Northeast Pacific include Al, V, Mn, Ni, Cu, Zn, As, Rb, Cd, and Pb. The final species listed above were determined using a filtering process like in MacDonald *et al.* (2020),[3] aiming for simplicity with fewer species of greater general interest while minimizing high covariance. For example, only Na^+ is used for sea salt, even though there were ample data on Cl^-.

As is customary in studies of this nature, charge balance analysis was conducted to understand how well the measured anions and cations balanced each other in terms of charge equivalent units (Fig. S1). The IC cations used included Na^+, NH_4^+, K^+, Mg^{2+}, and Ca^{2+}. The anions included are MSA, Cl^-, oxalate, NO_3^-, and SO_4^{2-}. With anions on the *y*-axis, the slopes were as follows: 1.01 (Northwest Atlantic), 0.99 (West Pacific), 0.98 (Northeast Pacific). Further analysis was conducted by computing the ratio (cations/anions) to understand the sensitivity of the charge balance on pH (Fig. S2). There is a general trend where pH values greater than 5 have a higher ratio, suggesting more cations are present at higher pH values. Lawrence *et al.* (2023)[27] showed for cloud water at Whiteface Mountain (New York) that nearly all samples with pH above 5.5 measured more cations than anions, which is similar to our results.

2.3 Calculations and modeling

2.3.1 Non-sea salt values. NSS-SO_4^{2-}, NSS-Ca^{2+}, and NSS-K^+ represent the non-sea salt fractions of SO_4^{2-}, Ca^{2+}, and K^+, respectively, calculated using Na^+ as a sea spray marker. The NSS fraction of SO_4^{2-} is calculated using eqn (1), where SO_4^{2-} is the total sulfate concentration. ssNa^+ is derived from sea spray, and 0.253 is the SO_4^{2-}/Na^+ ratio for seawater. NSS-Ca^{2+} is calculated using eqn (2), with Ca^{2+} representing total calcium and 0.038 being the Ca^{2+}/Na^+ ratio for sea water. NSS-K^+ is calculated using eqn (3), with 0.036 being the K^+/Na^+ ratio for seawater.[48,49]

$$\text{NSS} - SO_4^{2-} = SO_4^{2-} - (0.253x\ \text{ss}Na^+) \quad (1)$$

$$\text{NSS} - Ca^{2+} = Ca^{2+} - (0.038x\ \text{ss}Na^+) \quad (2)$$

$$\text{NSS} - K^+ = K^+ - (0.036x\ \text{ss}Na^+) \quad (3)$$

2.3.2 Gradient boosted regression tree modeling. To quantify the relationship between cloud water pH and chemical constituents, we used a gradient boosted regression tree (GBRT) model. GBRT uses a series of decision trees to build a predictive analysis, with each decision tree aiming to reduce the error from the previous one. In this study, we use pH as the dependent variable (or response variable), and the chemical constituents in aqueous concentration (mg L^{-1}) as the independent (or predictor) variables. GBRT provides feature importance scores and rankings to understand how much each chemical species influences the pH in the prediction model. The success of the regression was quantified using the coefficient of determination (R^2) and root mean squared error (RMSE).

2.3.3 Principal component analysis. Principal component analysis (PCA) is a technique used for dimensionality reduction.[50] We applied PCA to uncover relationships between chemical constituents and pH. The first principal component (PC1) captures the direction that describes the most variability in the data, while the second principal component (PC2) accounts for the highest degree of variability perpendicular to PC1. The results are then presented using explained variance and loading coefficients. Explained variance refers to the total variance in the data explained by a principal component. Loadings indicate the magnitude of a variable's contribution to a specific target value within that principal component.[51] In this study, the target value is pH.

3 Results and discussion

3.1 Cumulative statistics

Table 3 and Fig. 2 illustrate bulk pH statistics for each region, while Fig. S3 shows a frequency histogram of pH values for each region. For context in terms of pH data discussed below, the pH of pure deionized water in equilibrium with CO_2 is ~5.6.[52] The median pH of cloud water measured in each region varied between 4.40 and 5.17. The Northwest Atlantic pH ranged from 3.01 to 6.97, with Bermuda recording a lower median of 4.74 across the three Northwest Atlantic dataset categories. Previous airborne studies exhibit a similar range, but the median is higher than most studies in Table 1. Spatially, Northwest Atlantic samples show generally slightly higher pH values south of ~36°N, consistent with higher amounts of dust to the south, whereas farther north, there is generally more sulfate and organics.[53] Spatial maps of some influential species (Fig. S4) reveal high concentrations of NSS-Ca^{2+} corresponding to the higher pH values, consistent with higher amounts of dust to the south. Farther north, there are high concentrations of NSS-SO_4^{2-} and NO_3^- corresponding to the lower pH values. It is well documented that dust has alkaline constituents that can neutralize acidic ions (*e.g.*, sulfate and nitrate)[54,55] and thus elevate cloud and rainwater pH. The pH frequency histograms in Fig. S3 show how distinct Bermuda is in that it has no points below 4.5 with the narrowest pH range, likely due to its removal from large sources of acidic ions from major continental areas; a subset of those flights notably occurred during a period of African dust transport,[56,57] which can explain the very highest pH value of 5.93 in the Bermuda flights (Research Flight 170 on 10 June 2022) at the southernmost location around 30°N.

The West Pacific displayed the highest median pH value (5.17), which also exceeds values of previous airborne studies

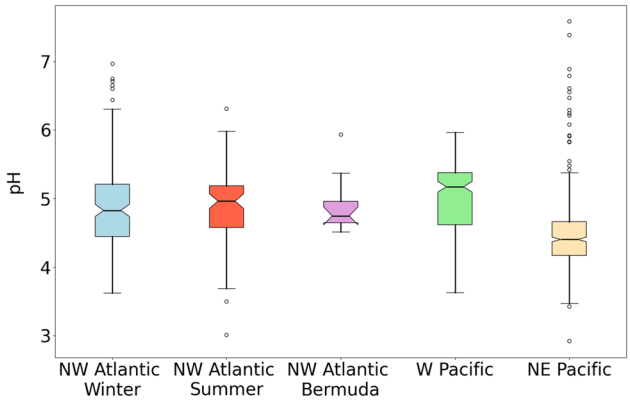

Fig. 2 The distribution of pH in each region is shown as a box-notched plot. The horizontal black line within the box represents the median value, and outliers are plotted as individual points beyond the whiskers. If the shaded notches do not overlap, this indicates that the medians are statistically different between the respective regions being compared.

(Table 1). There were no major spatial pH patterns of note in Fig. 1 other than how pH values over the ocean are lower than those near the Clark International Airport on the island of Luzon, Philippines. This could be due to high concentrations of NSS-SO_4^{2-}, NO_3^-, and oxalate farther from the Clark International Airport in areas with the lowest pH samples (Fig. S5).

The Northeast Pacific exhibited the widest pH range (2.92 to 7.58) and the lowest median pH (4.40) among the regions. This range is comparable to the range found in Benedict *et al.* (2012)[19] (Table 1), which examined similar types of stratocumulus clouds next to a major continental coast with sulfur emissions. The highest pH values over the Northeast Pacific were north of San Francisco and linked to continental air masses, whereas some of the lowest pH values were south of San Francisco, which is a bustling area for ship traffic and sulfur emissions.[20,58] This is consistent with Fig. S6, which shows NSS-SO_4^{2-}, oxalate, and NO_3^- having high concentrations in that area.

Comparing the median pH between the categories, which is visually illustrated by the box notch plots (see the caption of Fig. 2), the West Pacific and Northeast Pacific are both different than all other categories. In contrast, the three Northwest Atlantic categories were statistically similar to one another with intermediate values compared to the other two regions.

Fig. 3 depicts vertical profiles of the median pH in each region, and Fig. S7 shows the number of data points in each

Table 3 Statistical results for pH from the three study regions, with Northwest Atlantic divided into ACTIVATE's seasonal deployments and the Bermuda intensive period in June 2022

Region	Average	Median	25th %	75th %	Min	Max
Northwest Atlantic winter ($n = 178$)	4.87	4.83	4.44	5.21	3.62	6.97
Northwest Atlantic summer ($n = 79$)	4.94	4.96	4.63	5.18	3.01	6.31
Northwest Atlantic Bermuda ($n = 14$)	4.87	4.74	4.65	4.96	4.51	5.93
West Pacific ($n = 238$)	5.02	5.17	4.62	5.38	3.63	5.96
Northeast Pacific ($n = 517$)	4.46	4.40	4.17	4.66	2.92	7.58

vertical bin. Beginning with Northwest Atlantic samples, the winter generally showed a narrow range of medians from 4.5 to 5.0 from 120 to 3000 m. In contrast, the summer showed a more pronounced increase from 4.8 to 5.9 up to 1.5 km before the pH dropped gradually to 4.3 at 3.0 km. Bermuda samples, albeit only 14 in total, showed a narrow range across the altitude range of sample collection. Thus, the summertime showed the most vertical variability, which is seasonally consistent with a higher frequency of episodic events such as biomass burning and dust transport.[59,60] This is consistent when analyzing vertical profiles of influential species such as NSS-Ca^{2+}, NSS-SO_4^{2-}, and NO_3^-. There is an increase up to 1.5 km in NSS-Ca^{2+} before it decreases, which coincides with the increase in pH at that altitude (Fig. S8). NSS-SO_4^{2-} and NO_3^- show high concentrations between 2.5 and 3.0 km, coinciding with the gradual decrease in pH and the lower pH value (4.3) at 3.0 km (Fig. S9 and S10). The West Pacific samples were collected as high as 6.8 km, and the median pH generally increased with altitude, which corresponds with vertical profiles of NSS-SO_4^{2-} and NO_3^- that decrease with altitude (Fig. S9 and S10). The Northeast Pacific samples were all confined below 1 km due to the lower altitude of the sampled stratocumulus clouds relative to other regions with different cloud types. The median pH was generally between 4 and 5. NSS-Ca^{2+}, NSS-SO_4^{2-}, and NO_3^- showed similar vertical variability to each other in this region with decreasing concentrations as a function of altitude (Fig. S8–S10).

3.2 pH relationship with species

3.2.1 Principal component analysis. We used PCA to understand the relationships between cloud water pH and speciated constituents, as summarized in Table 2. We focused on results based solely on IC species (Fig. 4), with a separate set of results in Fig. S11 when ICP-MS species were added to the Northeast Pacific and Northwest Atlantic. Combining the first three principal components explains 67% of the total variance in the Northwest Atlantic, 85% over the West Pacific, and 76% over the Northeast Pacific. Therefore, the first three principal components were deemed sufficient for explaining the relationship between pH and the chemical constituents. The

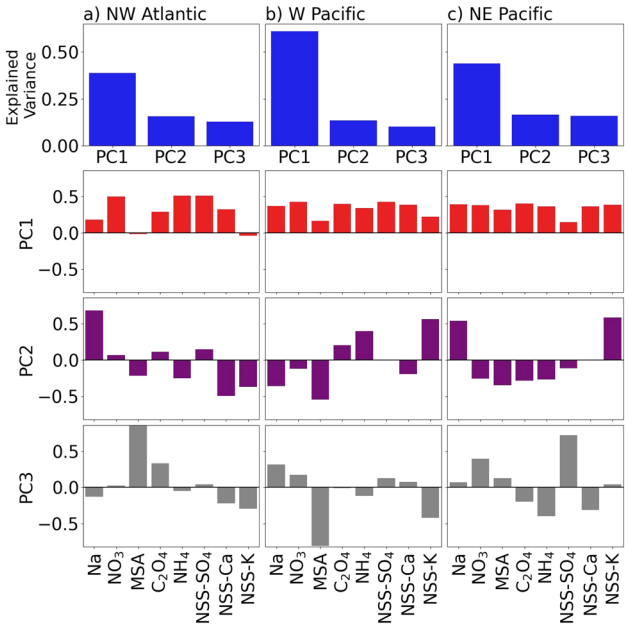

Fig. 4 Principal Component Analysis (PCA) plots of explained variance (first row) and loadings (succeeding rows) for (a)–(c) each region. Principal component 1 (PC1) describes the most variance in the data, and PC2 explains the second most variance and is orthogonal to PC1. Each loading represents its contribution to that PC.

bottom panels shown in Fig. 4 illustrate the loadings and their coefficients for each principal component. The highest loading value (*i.e.*, taller bar) in each principal component represents the species that holds the most useful information for that principal component.[51,61] Thus, if a PC has a high loading of a specific species, insights can be gathered about the potential sources impacting the region based on documented sources of that species. The sign of the loading (positive or negative) indicates the direction of the correlation with the species and the principal component. The magnitude of the loading is more important than the sign of the loading.

For context, previous work on cloud water collected at Mt. Mitchell (see Table 1) employed PCA to investigate the relationship between cloud water and air mass sources. The air

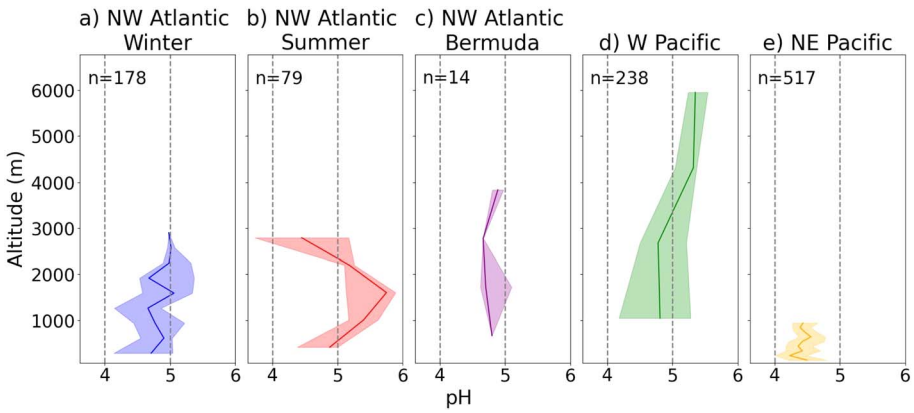

Fig. 3 Median pH as a function of altitude for (a)–(c) Northwest Atlantic, (d) West Pacific, and (e) Northeast Pacific. The shaded area denotes the 25th and 75th percentiles. The Northwest Atlantic is divided into seasons: (a) winter, (b) summer, and (c) summer Bermuda.

mass sources were characterized into three sectors: highly polluted, polluted marine, and polluted continental, using back trajectories computed by HYSPLIT. PCA was able to explain why the pH was so acidic under polluted marine conditions (average of 3.29); while their first two PCs were representative of sea spray (high loadings for Na^+, K^+, Mg^{2+}, Ca^{2+}, and Cl^-), their PC3 suggested the presence of KCl and HCl, which can account for the lower pH.[25] Another study at the Puy de Dôme, France, used a hierarchical clustering analysis to identify four clusters. PCA was then used to identify the individual species influencing the clusters.[28] The clusters included "highly marine" characterized by high concentrations of Na^+ and Cl^-, "marine" with low concentrations of Na^+ and Cl^-, and "continental" and "polluted" coincident with high levels of NH_4^+, NO_3^-, and SO_4^{2-}. From these clusters, they found the median pH to be the lowest (4.3) in the "polluted" clusters and the highest (6.2) in the "highly marine" cluster.

PC1 explains ~38% of the explained variance for the Northwest Atlantic. NO_3^-, NSS-SO_4^{2-}, and NH_4^+ demonstrated the highest loadings in PC1 (~0.50) and are linked to anthropogenic emissions and secondary aerosol formation processes in that region.[62] PC2 explains ~16% of the variance, where Na^+ had the highest loading of 0.69, suggesting sea spray influence. PC2 also had appreciable influence from NSS-Ca^{2+} (0.49) and NSS-K^+ (0.37), possibly suggesting roles for crustal sources and combustion.[11,62] PC3 explains ~13% of the explained variance, where MSA had the highest loading (~0.80), suggesting that biogenic emissions influence the pH since MSA is typically derived from ocean-emitted dimethylsulfide in marine regions.[63–65]

PC1 for the West Pacific explains ~61% of the total explained variance, with most species exhibiting high loadings, in particular, NO_3^-, oxalate, and NSS-SO_4^{2-}, suggesting that pH was affected by anthropogenic emissions such as exhaust, fossil fuel combustion, and biomass burning.[66] PC2 explains ~13% of the explained variance, with MSA and NSS-K^+ having the highest loadings (~0.55), suggesting some combination of biomass burning and biogenic emissions. NSS-K^+ is a well-known biomass burning tracer, which was a prominent feature during West Pacific flights.[22,39,67,68] While MSA is traditionally noted to be derived from marine biogenic emissions, there are several reports suggesting that it is enriched in smoke plumes.[63,69] PC3 explains ~10% of the total variance, with MSA showing the highest coefficient (~0.80) followed by NSS-K^+. The combination of those two species is suggestive of a smoke source.

PC1 explains ~43% of the variance for the Northeast Pacific, with most species having high loadings except for NSS-SO_4^{2-}. This type of profile suggests sea spray and continental emissions. PC2 explains ~17% of the explained variance, with NSS-K^+ having the highest loading (~0.58), followed by Na^+ (~0.54). This suggests that pH is influenced by combustion and sea spray in PC2. PC3 explains ~16% of the explained variance, with NSS-SO_4^{2-} having the highest loading, suggestive of the influence of anthropogenic emissions, especially ship exhaust.

A separate PCA was performed for the Northwest Atlantic and Northeast Pacific, including IC and ICP-MS species, as shown in Fig. S11. The total explained variance in Fig. 4 for the Northwest Atlantic was ~67%, and in the Northeast Pacific it was ~75%. When adding the ICP-MS species to the analysis, the total explained variance for the Northwest Atlantic becomes ~55%, while for the Northeast Pacific it becomes ~59%. When adding the ICP-MS species to the analysis, the total explained variance decreases, suggesting less data variance is captured in the PCA. For the Northwest Atlantic, the PCA in Fig. 4a and S11a is consistent in that PC1 has the most substantial influence from anthropogenic emissions. However, there is less evidence of marine influence when the ICP-MS species are included. In the Northeast Pacific, the PCA in Fig. 4c and S11b is consistent in that anthropogenic emissions and sea spray influence PC1. It is concluded that the PCA is sufficient with IC species for the datasets used without any need for ICP-MS elemental composition data inputs.

3.2.2 Predictive analysis. We conducted a correlation bar plot and a predictive analysis using gradient boosting regression tree modeling to further investigate the relationship between chemical constituents and pH. The correlation bar plot displays the species highly correlated with pH in each region (Fig. 5, right column). For the Northwest Atlantic, oxalate, NO_3^-, and NSS-Ca^{2+} show the highest correlation coefficients (r) with pH (r: −0.30, −0.27, and 0.35), indicating that sources of anthropogenic emissions and dust are highly influential in predicting the pH. Similarly, over the West Pacific, oxalate, NO_3^-, and NSS-SO_4^{2-} demonstrate the strongest correlation with pH (r: −0.59, −0.51, and −0.63), implying that anthropogenic emissions are highly influential for pH predictions. The Northeast Pacific reveals the highest correlation of pH with MSA, NO_3^-, and NSS-Ca^{2+} (r: −0.20, −0.24, and 0.32), suggesting the influence of a mix of biogenic and anthropogenic emissions and dust.

To learn more about species interrelationships and possible sources and/or production pathways for species, Fig. S12 shows a correlation matrix of statistically significant values (p <0.05) between the pH and the chemical constituents. The Northwest Atlantic and Northeast Pacific include ICP-MS species in this matrix. Each region reveals that NO_3^- is a highly correlated and statistically significant species with pH (Fig. 5), which indicates the importance of understanding NO_3^- chemistry and emissions impacting cloud water in different regions. NO_3^- can alter the microphysical properties in clouds and act as an effective CCN.[21,70,71] For the Northwest Atlantic, NO_3^-, NH_4^+, and NSS-SO_4^{2-} are highly correlated (r: ~0.70), suggesting the presence of secondary produced species (Fig. S12). In the West Pacific and Northeast Pacific, NO_3^-, NH_4^+, NSS-SO_4^{2-}, and oxalate are highly correlated (r: ~0.47–0.88), also suggestive of secondary produced species. For the Northeast Pacific, NO_3^- exhibited different behavior with its highest correlations being with oxalate and nickel (Fig. S12). In addition to NO_3^-, other highly ranked species in the correlations of Fig. 5 include NSS-Ca^{2+} and oxalate. While NSS-Ca^{2+} is known to be an alkaline species enriched in dust that can enhance the pH, explaining its positive and highly ranked correlation with pH in at least two regions, it is interesting that oxalate emerges as a highly ranked species in the correlation bar plots. This species has a wide

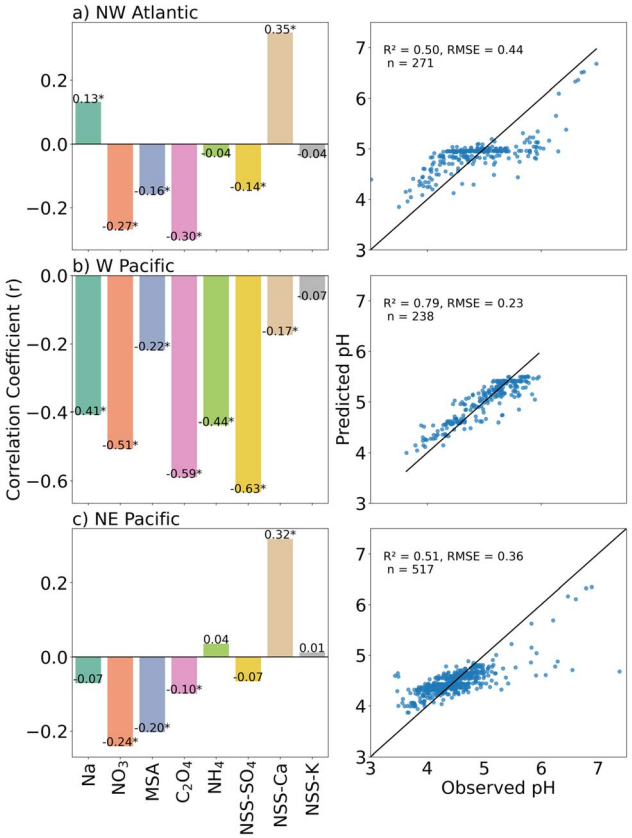

Fig. 5 (Left) Correlation bar plot showing the Pearson correlation coefficient (r) between the measured IC chemical species and measured pH for (a–c) each region. Statistically significant values ($p < 0.05$) are marked by an asterisk (*). Exact r values are shown on each bar. (Right) Scatterplots comparing the measured and predicted pH based on a GBRT model built with three influential species from the respective correlation bar plots in the left column. The GBRT model R^2 value, RMSE value, and number of points (n) used in the analysis are shown in the panels.

range of sources (*e.g.*, biogenic, anthropogenic, and biomass burning)[66,72] and known to be a product of aqueous secondary aerosol processing,[73,74] as supported by many studies in its correlation with sulfate,[68,75] which is evident for the Northwest Atlantic and West Pacific in Fig. S12. The lack of a statistically significant correlation between the two species for the Northeast Pacific may simply be due to the more pronounced correlations of oxalate with MSA, NO_3^-, and NSS-Ca^{2+}, suggesting that dust and possibly biomass burning were more influential sources of that species owing to some episodic events.[76,77] Overall, for the Northeast Pacific, Na^+ and NSS-K^+ are the most highly correlated pair of species ($r = 0.96$), suggestive of a high presence of sea salt in the region.

The most influential species mentioned above were then used in a predictive analysis using gradient boosting regression trees (GBRT) (Fig. 5, left column). Fig. 6 presents the feature importance of the species that are most influential to pH. The predictive analysis performed best for the West Pacific, achieving an R^2 of 0.79, while the Northwest Atlantic and Northeast Pacific had R^2 values of 0.50 and 0.51, respectively. For the Northwest Atlantic, the feature importance results revealed that NSS-Ca^{2+} was the most influential species for pH with a coefficient of 0.49, followed by NO_3^- (0.36) and oxalate (0.16). The feature importance results for the West Pacific showed that NSS-SO_4^{2-} significantly influenced the pH with a coefficient of 0.76, compared to oxalate and NO_3^- with coefficients of 0.14 and 0.11, respectively. In the Northeast Pacific, NO_3^- and NSS-Ca^{2+} exhibited similar importance with coefficients of 0.43 and 0.42, respectively, while MSA had much lower importance with a coefficient of 0.14.

To complement the model results and further our understanding of the relationship between these species and pH, Fig. S13 demonstrates scatterplots of the three species in each region that are highly correlated with pH. These scatterplots confirm the negative relationship for the more acidic species like oxalate and NO_3^-, and the positive relationship for NSS-Ca^{2+}, a more alkaline species. Fig. S14–S16 show scatterplots of pH *versus* all IC species for each region to confirm the relationship between basic and acidic species.

The predictive analyses are further interrogated to see how the difference between the observed and predicted pH (*i.e.*, the residual value) varies spatially (Fig. 7) and vertically (Fig. 8) for each region. A negative residual value indicates the observed pH is lower than the predicted pH, while a zero value means the

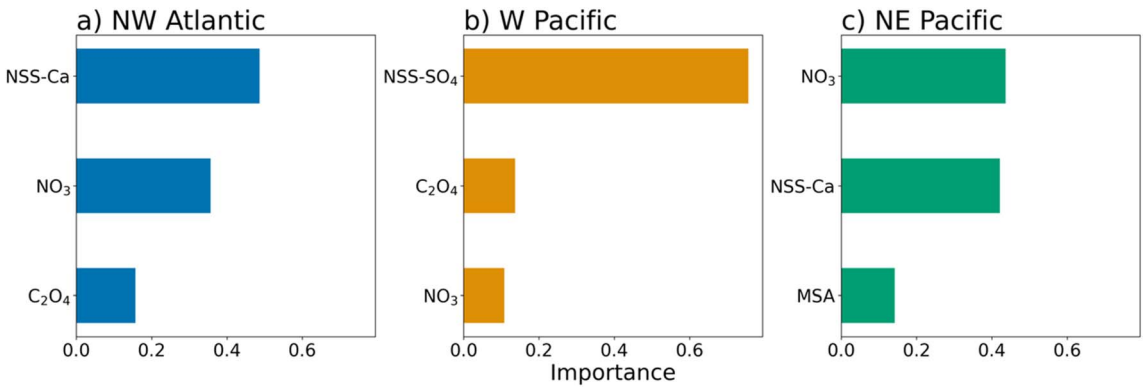

Fig. 6 Feature importance from the GBRT for the (a) Northwest Atlantic, (b) West Pacific, and (c) Northeast Pacific. The x-axis represents the importance value (coefficient) that is most influential to pH in the predictive analysis.

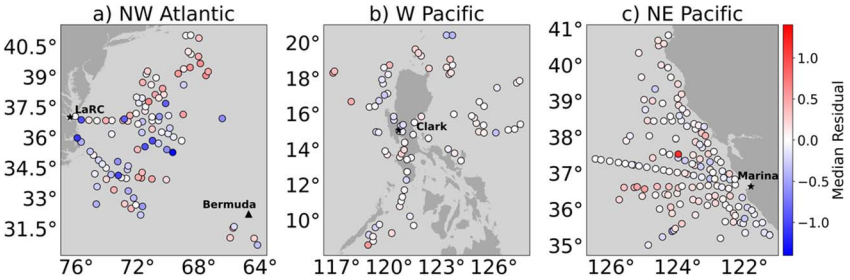

Fig. 7 Spatial maps of the predicted minus observed pH (*i.e.*, residual values) for the (a) Northwest Atlantic, (b) West Pacific, and (c) Northeast Pacific. Markers represent the median pH residual value calculated for that given pixel in the map. The predicted pH is determined from the GBRT analysis.

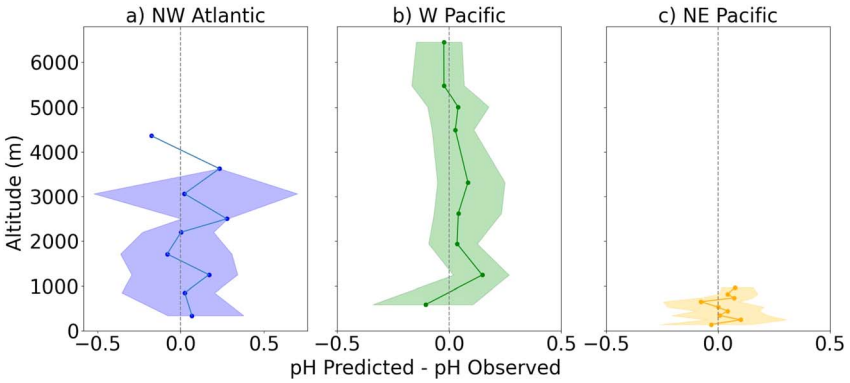

Fig. 8 Vertical profiles of median residual values calculated as the difference between the predicted and observed pH for the (a) Northwest Atlantic, (b) West Pacific, and (c) Northeast Pacific. The predicted pH is determined from the GBRT. The shaded regions indicate the 25th and 75th percentiles. A dashed vertical line is provided for a residual value of 0 (*i.e.*, predicted and observed values agree).

predicted and observed values are the same. Over the Northwest Atlantic, there is no clear offshore gradient. However, generally, there are more positive values to the north of 37°N. This is possibly due to the high influence of NSS-Ca^{2+} in the model, which is more prominent in the south. The Ca^{2+} ion is a good neutralizing component for cloud water acidity, and it is possible for more negative residuals to the south. For the West Pacific, there is a slight gradient with higher negative and positive values farther from the Clark International Airport, especially farther north where there is a greater presence of positive values. This is possibly because of too much influence on NSS-SO_4^{2-} in the model and the greater presence of smoke in the southern area of the study region, causing the predicted pH to be more acidic. In the Northeast Pacific, there is no clear offshore gradient. However, there is a greater presence of positive and zero values, indicating the model predicts pH well. Fig. 8 reveals no major sensitivity of residual values to altitude over all the regions. The median residual value for different vertical bins remains positive with altitude.

4 Conclusion

This work analyzed ≥230 cloud water samples in each of three diverse regions: the Northwest Atlantic, the West Pacific, and the Northeast Pacific. Samples were analyzed for pH and speciated ion and elemental species concentrations. Statistical analysis was performed for each region, with Bermuda samples exhibiting the lowest median pH (4.74) compared to winter (4.83) and summer (4.96) samples over the Northwest Atlantic. The West Pacific had the highest median pH (5.17) among the regions. The Northeast Pacific exhibited the region's broadest pH range (2.92–7.58) and lowest median pH (4.40) owing to suspected large influence from shipping exhaust enriched with sulfur constituents.

From the IC species collected during the research flights, 8 species were selected through a filtering process to investigate which species significantly influence the pH in each region. With some exceptions based on region, correlation analysis showed that pH was most negatively correlated with NO_3^-, NSS-SO_4^{2-}, and oxalate, while it was most positively correlated with NSS-Ca^{2+}. PCA results indicated that in all regions, PC1 suggested the presence of anthropogenic emissions based on the influence of species such as NO_3^-, NSS-SO_4^{2-}, and NH_4^+. The less influential components (PC2–PC3) had source profiles suggestive of some combination of biomass burning, sea spray, and biogenic emissions. GBRT analysis using three predictor species for pH in each region revealed the best performance for the West Pacific, achieving an R^2 of 0.79. The R^2 in the Northwest Atlantic was 0.50, while in the Northeast Pacific it was 0.51. These models were based on inputs being some combination of oxalate, NO_3^-, NSS-SO_4^{2-}, MSA, and NSS-Ca^{2+}. The feature

importance of these species found that in the Northwest Atlantic, NSS-Ca^{2+} exhibited the highest importance with a coefficient of 0.49, followed by NO_3^- (0.36) and oxalate (0.16). In the West Pacific, the feature importance showed NSS-SO_4^{2-} (coefficient of 0.76) significantly influencing the pH, compared to oxalate (0.14) and NO_3^- (0.11). In the Northeast Pacific, NO_3^- (0.43) and NSS-Ca^{2+} (0.42) showed similar importance, compared to MSA (0.14), which was much lower. In further investigating the predictive models, the residual value (predicted-observed pH) was calculated and interpreted spatially and vertically, pointing to some differences likely due to the high influence of some species in the models that have spatial and vertical gradients.

In general, the results show that pH is generally well constrained between 4 and 5.5 and that anthropogenic activities consistently act to reduce pH in all regions, but this can be offset by dust during episodic events. This has implications for atmospheric chemistry and effects on human health and ecosystems. Future work is warranted to study cloud water pH and its most influential species for other unexplored regions.

Author contributions

KMP conducted the data analysis and drafted the original manuscript. ECC, MRAH, GB, RAB, AFC, EE, ABM, AHM, MAS, CS, ELW, KZ, LDZ, and AS contributed to data collection and processing. AS acquired funding. All authors contributed to discussion, review, and editing of the manuscript. All authors have approved the final version of the manuscript.

Conflicts of interest

There are no conflicts to declare.

Data availability

ACTIVATE airborne data can be obtained at **https://doi.org/10.5067/SUBORBITAL/ACTIVATE/DATA001**. CAMP^{2}Ex data can be obtained at **https://doi.org/10.5067/Airborne/CAMP2Ex_Aerosol_AircraftInSitu_P3_Data_1**. Northeast Pacific data can be obtained at **https://doi.org/10.6084/m9.figshare.5099983.v11**.

Supplementary information is available. See DOI: **https://doi.org/10.1039/d5ea00070j**.

Acknowledgements

We acknowledge the pilots and aircraft maintenance personnel of NASA Langley Research Services Directorate for successfully conducting ACTIVATE flights and all others involved in executing the campaign. This work was funded by ACTIVATE, a NASA Earth Venture Suborbital-3 (EVS-3) investigation funded by NASA's Earth Science Division and managed through the Earth System Science Pathfinder Program Office. The University of Arizona investigators were funded by NASA grant numbers 80NSSC19K0442 and 80NSSC18K0148 and ONR grant number N00014-21-1-2115.

References

1 Z. Wang, M. Mora Ramirez, H. Dadashazar, A. B. MacDonald, E. Crosbie, K. H. Bates, M. M. Coggon, J. S. Craven, P. Lynch, J. R. Campbell, M. Azadi Aghdam, R. K. Woods, H. Jonsson, R. C. Flagan, J. H. Seinfeld and A. Sorooshian, Contrasting cloud composition between coupled and decoupled marine boundary layer clouds, *J. Geophys. Res.:Atmos.*, 2016, **121**(11), 611–691.

2 H. O. T. Pye, A. Nenes, B. Alexander, A. P. Ault, M. C. Barth, S. L. Clegg, J. L. Collett Jr, K. M. Fahey, C. J. Hennigan, H. Herrmann, M. Kanakidou, J. T. Kelly, I. T. Ku, V. F. McNeill, N. Riemer, T. Schaefer, G. Shi, A. Tilgner, J. T. Walker, T. Wang, R. Weber, J. Xing, R. A. Zaveri and A. Zuend, The acidity of atmospheric particles and clouds, *Atmos. Chem. Phys.*, 2020, **20**, 4809–4888.

3 A. B. MacDonald, A. Hossein Mardi, H. Dadashazar, M. Azadi Aghdam, E. Crosbie, H. H. Jonsson, R. C. Flagan, J. H. Seinfeld and A. Sorooshian, On the relationship between cloud water composition and cloud droplet number concentration, *Atmos. Chem. Phys.*, 2020, **20**, 7645–7665.

4 R. J. Charlson, S. E. Schwartz, J. M. Hales, R. D. Cess, J. A. Coakley, J. E. Hansen and D. J. Hofmann, Climate Forcing by Anthropogenic Aerosols, *Science*, 1992, **255**, 423–430.

5 J. L. Collett Jr, A. Bator, X. Rao and B. B. Demoz, Acidity variations across the cloud drop size spectrum and their influence on rates of atmospheric sulfate production, *Geophys. Res. Lett.*, 1994, **21**, 2393–2396.

6 Y.-H. Ryu and S.-K. Min, Long-term evaluation of atmospheric composition reanalyses from CAMS, TCR-2, and MERRA-2 over South Korea: Insights into applications, implications, and limitations, *Atmos. Environ.*, 2021, **246**, 118062.

7 A. Roy, A. Chatterjee, A. Ghosh, S. K. Das, S. K. Ghosh and S. Raha, Below-cloud scavenging of size-segregated aerosols and its effect on rainwater acidity and nutrient deposition: A long-term (2009–2018) and real-time observation over eastern Himalaya, *Sci. Total Environ.*, 2019, **674**, 223–233.

8 A. B. MacDonald, H. Dadashazar, P. Y. Chuang, E. Crosbie, H. Wang, Z. Wang, H. H. Jonsson, R. C. Flagan, J. H. Seinfeld and A. Sorooshian, Characteristic Vertical Profiles of Cloud Water Composition in Marine Stratocumulus Clouds and Relationships With Precipitation, *J. Geophys. Res.:Atmos.*, 2018, **123**, 3704–3723.

9 K. Zeider, K. McCauley, S. Dmitrovic, L. W. Siu, Y. Choi, E. C. Crosbie, J. P. DiGangi, G. S. Diskin, S. Kirschler, J. B. Nowak, M. A. Shook, K. L. Thornhill, C. Voigt, E. L. Winstead, L. D. Ziemba, P. Zuidema and A. Sorooshian, Sensitivity of aerosol and cloud properties to coupling strength of marine boundary layer clouds over the northwest Atlantic, *Atmos. Chem. Phys.*, 2025, **25**, 2407–2422.

10 V. Shah, D. J. Jacob, J. M. Moch, X. Wang and S. Zhai, Global modeling of cloud water acidity, precipitation acidity, and

acid inputs to ecosystems, *Atmos. Chem. Phys.*, 2020, **20**, 12223–12245.

11 A. Gioda, G. J. Reyes-Rodríguez, G. Santos-Figueroa, J. L. Collett Jr, S. Decesari, M. d. C. K. V. Ramos, H. J. C. Bezerra Netto, F. R. de Aquino Neto and O. L. Mayol-Bracero, Speciation of water-soluble inorganic, organic, and total nitrogen in a background marine environment: Cloud water, rainwater, and aerosol particles, *J. Geophys. Res.:Atmos.*, 2011, **116**, D05203.

12 K. B. Budhavant, P. S. P. Rao, P. D. Safai, L. Granat and H. Rodhe, Chemical composition of the inorganic fraction of cloud-water at a high altitude station in West India, *Atmos. Environ.*, 2014, **88**, 59–65.

13 M. Sun, Y. Wang, T. Wang, S. Fan, W. Wang, P. Li, J. Guo and Y. Li, Cloud and the corresponding precipitation chemistry in south China: Water-soluble components and pollution transport, *J. Geophys. Res.:Atmos.*, 2010, **115**, D22303.

14 T. Li, Z. Wang, Y. Wang, C. Wu, Y. Liang, M. Xia, C. Yu, H. Yun, W. Wang, Y. Wang, J. Guo, H. Herrmann and T. Wang, Chemical characteristics of cloud water and the impacts on aerosol properties at a subtropical mountain site in Hong Kong SAR, *Atmos. Chem. Phys.*, 2020, **20**, 391–407.

15 F. Parungo, C. Nagamoto, I. Nolt, M. Dias and E. Nickerson, Chemical analysis of cloud water collected over Hawaii, *J. Geophys. Res.:Oceans*, 1982, **87**, 8805–8810.

16 K. Watanabe, Y. Ishizaka and C. Takenaka, Chemical characteristics of cloud water over the Japan Sea and the Northwestern Pacific Ocean near the central part of Japan: airborne measurements, *Atmos. Environ.*, 2001, **35**, 645–655.

17 D. J. Straub, T. Lee and J. L. Collett Jr, Chemical composition of marine stratocumulus clouds over the eastern Pacific Ocean, *J. Geophys. Res.:Atmos.*, 2007, **112**, D04307.

18 K. A. Hill, P. B. Shepson, E. S. Galbavy, C. Anastasio, P. S. Kourtev, A. Konopka and B. H. Stirm, Processing of atmospheric nitrogen by clouds above a forest environment, *J. Geophys. Res.:Atmos.*, 2007, **112**, D11301.

19 K. B. Benedict, T. Lee and J. L. Collett, Cloud water composition over the southeastern Pacific Ocean during the VOCALS regional experiment, *Atmos. Environ.*, 2012, **46**, 104–114.

20 Z. Wang, A. Sorooshian, G. Prabhakar, M. M. Coggon and H. H. Jonsson, Impact of emissions from shipping, land, and the ocean on stratocumulus cloud water elemental composition during the 2011 E-PEACE field campaign, *Atmos. Environ.*, 2014, **89**, 570–580.

21 G. Prabhakar, B. Ervens, Z. Wang, L. C. Maudlin, M. M. Coggon, H. H. Jonsson, J. H. Seinfeld and A. Sorooshian, Sources of nitrate in stratocumulus cloud water: Airborne measurements during the 2011 E-PEACE and 2013 NiCE studies, *Atmos. Environ.*, 2014, **97**, 166–173.

22 C. Stahl, E. Crosbie, P. A. Bañaga, G. Betito, R. A. Braun, Z. M. Cainglet, M. O. Cambaliza, M. T. Cruz, J. M. Dado, M. R. A. Hilario, G. F. Leung, A. B. MacDonald, A. M. Magnaye, J. Reid, C. Robinson, M. A. Shook, J. B. Simpas, S. M. Visaga, E. Winstead, L. Ziemba and A. Sorooshian, Total organic carbon and the contribution from speciated organics in cloud water: airborne data analysis from the CAMP2Ex field campaign, *Atmos. Chem. Phys.*, 2021, **21**, 14109–14129.

23 B. T. Bormann, R. F. Tarrant, M. H. McClellan and T. Savage, Chemistry of Rainwater and Cloud Water at Remote Sites in Alaska and Oregon, *J. Environ. Qual.*, 1989, **18**, 149–152.

24 G. L. D. Murray, K. D. Kimball, L. B. Hill, J. E. Hislop and K. C. Weathers, Long-Term Trends in Cloud and Rain Chemistry on Mount Washington, New Hampshire, *Water, Air, Soil Pollut.*, 2013, **224**, 1653.

25 C. K. Deininger and V. K. Saxena, A validation of back trajectories of air masses by principal component analysis of ion concentrations in cloud water, *Atmos. Environ.*, 1997, **31**, 295–300.

26 R. J. Vong, B. M. Baker, F. J. Brechtel, R. T. Collier, J. M. Harris, A. S. Kowalski, N. C. McDonald and L. M. McInnes, Ionic and trace element composition of cloud water collected on the Olympic Peninsula of Washington State, *Atmos. Environ.*, 1997, **31**, 1991–2001.

27 C. E. Lawrence, P. Casson, R. Brandt, J. J. Schwab, J. E. Dukett, P. Snyder, E. Yerger, D. Kelting, T. C. VandenBoer and S. Lance, Long-term monitoring of cloud water chemistry at Whiteface Mountain: the emergence of a new chemical regime, *Atmos. Chem. Phys.*, 2023, **23**, 1619–1639.

28 L. Deguillaume, T. Charbouillot, M. Joly, M. Vaïtilingom, M. Parazols, A. Marinoni, P. Amato, A. M. Delort, V. Vinatier, A. Flossmann, N. Chaumerliac, J. M. Pichon, S. Houdier, P. Laj, K. Sellegri, A. Colomb, M. Brigante and G. Mailhot, Classification of clouds sampled at the puy de Dôme (France) based on 10 yr of monitoring of their physicochemical properties, *Atmos. Chem. Phys.*, 2014, **14**, 1485–1506.

29 J. W. Hutchings, M. S. Robinson, H. McIlwraith, J. Triplett Kingston and P. Herckes, The Chemistry of Intercepted Clouds in Northern Arizona during the North American Monsoon Season, *Water, Air, Soil Pollut.*, 2009, **199**, 191–202.

30 J. Guo, Y. Wang, X. Shen, Z. Wang, T. Lee, X. Wang, P. Li, M. Sun, J. L. Collett, W. Wang and T. Wang, Characterization of cloud water chemistry at Mount Tai, China: Seasonal variation, anthropogenic impact, and cloud processing, *Atmos. Environ.*, 2012, **60**, 467–476.

31 D. van Pinxteren, K. W. Fomba, S. Mertes, K. Müller, G. Spindler, J. Schneider, T. Lee, J. L. Collett and H. Herrmann, Cloud water composition during HCCT-2010: Scavenging efficiencies, solute concentrations, and droplet size dependence of inorganic ions and dissolved organic carbon, *Atmos. Chem. Phys.*, 2016, **16**, 3185–3205.

32 L. Sun, Y. Wang, T. Yue, X. Yang, L. Xue and W. Wang, Evaluation of the behavior of clouds in a region of severe acid rain pollution in southern China: species, complexes, and variations, *Environ. Sci. Pollut. Res.*, 2015, **22**, 14280–14290.

33 J. Li, X. Wang, J. Chen, C. Zhu, W. Li, C. Li, L. Liu, C. Xu, L. Wen, L. Xue, W. Wang, A. Ding and H. Herrmann, Chemical composition and droplet size distribution of

cloud at the summit of Mount Tai, China, *Atmos. Chem. Phys.*, 2017, **17**, 9885–9896.

34 C. Zhu, J. Chen, X. Wang, J. Li, M. Wei, C. Xu, X. Xu, A. Ding and J. J. L. Collett, Chemical Composition and Bacterial Community in Size-Resolved Cloud Water at the Summit of Mt. Tai, China, *Aerosol Air Qual. Res.*, 2018, **18**, 1–14.

35 X. Sun, Y. Wang, H. Li, X. Yang, L. Sun, X. Wang, T. Wang and W. Wang, Organic acids in cloud water and rainwater at a mountain site in acid rain areas of South China, *Environ. Sci. Pollut. Res. Int.*, 2016, **23**, 9529.

36 A. Sorooshian, B. Anderson, S. E. Bauer, R. A. Braun, B. Cairns, E. Crosbie, H. Dadashazar, G. Diskin, R. Ferrare, R. C. Flagan, J. Hair, C. Hostetler, H. H. Jonsson, M. M. Kleb, H. Liu, A. B. MacDonald, A. McComiskey, R. Moore, D. Painemal, L. M. Russell, J. H. Seinfeld, M. Shook, W. L. Smith, K. Thornhill, G. Tselioudis, H. Wang, X. Zeng, B. Zhang, L. Ziemba and P. Zuidema, Aerosol–Cloud–Meteorology Interaction Airborne Field Investigations: Using Lessons Learned from the U.S. West Coast in the Design of ACTIVATE off the U.S. East Coast, *Bull. Am. Meteorol. Soc.*, 2019, **100**, 1511–1528.

37 A. Sorooshian, M. D. Alexandrov, A. D. Bell, R. Bennett, G. Betito, S. P. Burton, M. E. Buzanowicz, B. Cairns, E. V. Chemyakin, G. Chen, Y. Choi, B. L. Collister, A. L. Cook, A. F. Corral, E. C. Crosbie, B. van Diedenhoven, J. P. DiGangi, G. S. Diskin, S. Dmitrovic, E. L. Edwards, M. A. Fenn, R. A. Ferrare, D. van Gilst, J. W. Hair, D. B. Harper, M. R. A. Hilario, C. A. Hostetler, N. Jester, M. Jones, S. Kirschler, M. M. Kleb, J. M. Kusterer, S. Leavor, J. W. Lee, H. Liu, K. McCauley, R. H. Moore, J. Nied, A. Notari, J. B. Nowak, D. Painemal, K. E. Phillips, C. E. Robinson, A. J. Scarino, J. S. Schlosser, S. T. Seaman, C. Seethala, T. J. Shingler, M. A. Shook, K. A. Sinclair, W. L. Smith Jr, D. A. Spangenberg, S. A. Stamnes, K. L. Thornhill, C. Voigt, H. Vömel, A. P. Wasilewski, H. Wang, E. L. Winstead, K. Zeider, X. Zeng, B. Zhang, L. D. Ziemba and P. Zuidema, Spatially coordinated airborne data and complementary products for aerosol, gas, cloud, and meteorological studies: the NASA ACTIVATE dataset, *Earth Syst. Sci. Data*, 2023, **15**, 3419–3472.

38 E. Crosbie, M. D. Brown, M. Shook, L. Ziemba, R. H. Moore, T. Shingler, E. Winstead, K. L. Thornhill, C. Robinson, A. B. MacDonald, H. Dadashazar, A. Sorooshian, A. Beyersdorf, A. Eugene, J. Collett Jr, D. Straub and B. Anderson, Development and characterization of a high-efficiency, aircraft-based axial cyclone cloud water collector, *Atmos. Meas. Tech.*, 2018, **11**, 5025–5048.

39 J. S. Reid, H. B. Maring, G. T. Narisma, S. van den Heever, L. Di Girolamo, R. Ferrare, P. Lawson, G. G. Mace, J. B. Simpas, S. Tanelli, L. Ziemba, B. van Diedenhoven, R. Bruintjes, A. Bucholtz, B. Cairns, M. O. Cambaliza, G. Chen, G. S. Diskin, J. H. Flynn, C. A. Hostetler, R. E. Holz, T. J. Lang, K. S. Schmidt, G. Smith, A. Sorooshian, E. J. Thompson, K. L. Thornhill, C. Trepte, J. Wang, S. Woods, S. Yoon, M. Alexandrov, S. Alvarez, C. G. Amiot, J. R. Bennett, M. Brooks, S. P. Burton, E. Cayanan, H. Chen, A. Collow, E. Crosbie, A. DaSilva, J. P. DiGangi, D. D. Flagg, S. W. Freeman, D. Fu, E. Fukada, M. R. A. Hilario, Y. Hong, S. M. Hristova-Veleva, R. Kuehn, R. S. Kowch, G. R. Leung, J. Loveridge, K. Meyer, R. M. Miller, M. J. Montes, J. N. Moum, A. Nenes, S. W. Nesbitt, M. Norgren, E. P. Nowottnick, R. M. Rauber, E. A. Reid, S. Rutledge, J. S. Schlosser, T. T. Sekiyama, M. A. Shook, G. A. Sokolowsky, S. A. Stamnes, T. Y. Tanaka, A. Wasilewski, P. Xian, Q. Xiao, Z. Xu and J. Zavaleta, The Coupling Between Tropical Meteorology, Aerosol Lifecycle, Convection, and Radiation during the Cloud, Aerosol and Monsoon Processes Philippines Experiment (CAMP2Ex), *Bull. Am. Meteorol. Soc.*, 2023, **104**, E1179–E1205.

40 E. Crosbie, L. D. Ziemba, M. A. Shook, C. E. Robinson, E. L. Winstead, K. L. Thornhill, R. A. Braun, A. B. MacDonald, C. Stahl, A. Sorooshian, S. C. van den Heever, J. P. DiGangi, G. S. Diskin, S. Woods, P. Bañaga, M. D. Brown, F. Gallo, M. R. A. Hilario, C. E. Jordan, G. R. Leung, R. H. Moore, K. J. Sanchez, T. J. Shingler and E. B. Wiggins, Measurement report: Closure analysis of aerosol–cloud composition in tropical maritime warm convection, *Atmos. Chem. Phys.*, 2022, **22**, 13269–13302.

41 A. Sorooshian, A. B. Macdonald, H. Dadashazar, K. H. Bates, M. M. Coggon, J. S. Craven, E. Crosbie, S. P. Hersey, N. Hodas, J. J. Lin, A. Negrón Marty, L. C. Maudlin, A. R. Metcalf, S. M. Murphy, L. T. Padró, G. Prabhakar, T. A. Rissman, T. Shingler, V. Varutbangkul, Z. Wang, R. K. Woods, P. Y. Chuang, A. Nenes, H. H. Jonsson, R. C. Flagan and J. H. Seinfeld, A multi-year data set on aerosol-cloud-precipitation-meteorology interactions for marine stratocumulus clouds, *Sci. Data*, 2018, **5**, 180026.

42 D. e. A. Hegg and P. V. Hobbs, Sulfate and nitrate chemistry in cumuliform clouds, *Atmos. Environ.*, 1986, **20**, 901–909.

43 D. J. Straub and J. L. Collett, An Axial-Flow Cyclone for Aircraft-Based Cloud Water Sampling, *J. Atmos. Ocean. Technol.*, 2004, **21**, 1825–1839.

44 B. J. Huebert and D. Baumgardner, A preliminary evaluation of the Mohnen slotted-rod cloud water collector, *Atmos. Environ.*, 1985, **19**, 843–846.

45 Y. J. Kim and J. F. Boatman, The Collection Efficiency of a Modified Mohnen Slotted-Rod Cloud-Water Collector in Summer Clouds, *J. Atmos. Ocean. Technol.*, 1992, **9**, 35–41.

46 K. Zeider, G. Betito, A. Bucholtz, P. Xian, A. Walker and A. Sorooshian, Differences in aerosol and cloud properties along the central California coast when winds change from northerly to southerly, *Atmos. Chem. Phys.*, 2024, **24**, 9059–9083.

47 A. B. M. Armin Sorooshian, H. Dadashazar, K. H. Bates, M. Coggon, J. S. Craven, E. Crosbie, S. P. Hersey, N. Hodas, J. J. Lin, A. Negrón Marty, Contributor L. C. Maudlin, A. R. Metcalf, S. M. Murphy. L. T. Padro, G. Prabhakar, T. A. Rissman, T. Shingler, V. Varutbangkul, Z. Wang, R. K. Woods, P. Y. Chuang, A. Nenes, H. Jonsson, R. C. Flagan, J. H. Seinfeld, *A Multi-Year Data Set on Aerosol-Cloud-Precipitation-Meteorology Interactions for Marine Stratocumulus Clouds*, figshare, 2018, DOI: **10.6084/m9.figshare.5099983.v8**.

48 S. Becagli, M. Proposito, S. Benassai, R. Gragnani, O. Magand, R. Traversi and R. Udisti, Spatial distribution of biogenic sulphur compounds (MSA, nssSO42–) in the northern Victoria Land–Dome C–Wilkes Land area, East Antarctica, *Ann. Glaciol.*, 2005, **41**, 23–31.

49 M. AzadiAghdam, R. A. Braun, E.-L. Edwards, P. A. Bañaga, M. T. Cruz, G. Betito, M. O. Cambaliza, H. Dadashazar, G. R. Lorenzo, L. Ma, A. B. MacDonald, P. Nguyen, J. B. Simpas, C. Stahl and A. Sorooshian, On the nature of sea salt aerosol at a coastal megacity: Insights from Manila, Philippines in Southeast Asia, *Atmos. Environ.*, 2019, **216**, 116922.

50 G. W. Petty, Physical and Microwave Radiative Properties of Precipitating Clouds. Part I: Principal Component Analysis of Observed Multichannel Microwave Radiances in Tropical Stratiform Rainfall, *J. Appl. Meteorol.*, 2001, **40**, 2105–2114.

51 S. Wold, K. Esbensen and P. Geladi, Principal component analysis, *Chemom. Intell. Lab. Syst.*, 1987, **2**, 37–52.

52 R. J. Charlson and H. Rodhe, Factors controlling the acidity of natural rainwater, *Nature*, 1982, **295**, 683–685.

53 A. F. Corral, R. A. Braun, B. Cairns, V. A. Gorooh, H. Liu, L. Ma, A. H. Mardi, D. Painemal, S. Stamnes, B. van Diedenhoven, H. Wang, Y. Yang, B. Zhang and A. Sorooshian, An Overview of Atmospheric Features Over the Western North Atlantic Ocean and North American East Coast – Part 1: Analysis of Aerosols, Gases, and Wet Deposition Chemistry, *J. Geophys. Res.:Atmos.*, 2021, **126**, e2020JD032592.

54 R. Arimoto, R. A. Duce, D. L. Savoie and J. M. Prospero, Trace elements in aerosol particles from Bermuda and Barbados: Concentrations, sources and relationships to aerosol sulfate, *J. Atmos. Chem.*, 1992, **14**, 439–457.

55 D. R. Muhs, J. R. Budahn, J. M. Prospero, G. Skipp and S. R. Herwitz, Soil genesis on the island of Bermuda in the Quaternary: The importance of African dust transport and deposition, *J. Geophys. Res.:Earth Surf.*, 2012, **117**, F03025.

56 T. Ajayi, Y. Choi, E. C. Crosbie, J. P. DiGangi, G. S. Diskin, M. A. Fenn, R. A. Ferrare, J. W. Hair, M. R. A. Hilario, C. A. Hostetler, S. Kirschler, R. H. Moore, T. J. Shingler, M. A. Shook, C. Soloff, K. L. Thornhill, C. Voigt, E. L. Winstead, L. D. Ziemba and A. Sorooshian, Vertical variability of aerosol properties and trace gases over a remote marine region: a case study over Bermuda, *Atmos. Chem. Phys.*, 2024, **24**, 9197–9218.

57 E. Crosbie, L. D. Ziemba, M. A. Shook, T. Shingler, J. W. Hair, A. Sorooshian, R. A. Ferrare, B. Cairns, Y. Choi, J. DiGangi, G. S. Diskin, C. Hostetler, S. Kirschler, R. H. Moore, D. Painemal, C. Robinson, S. T. Seaman, K. L. Thornhill, C. Voigt and E. Winstead, Measurement report: Cloud and environmental properties associated with aggregated shallow marine cumulus and cumulus congestus, *Atmos. Chem. Phys.*, 2024, **24**, 6123–6152.

58 M. M. Coggon, A. Sorooshian, Z. Wang, A. R. Metcalf, A. A. Frossard, J. J. Lin, J. S. Craven, A. Nenes, H. H. Jonsson, L. M. Russell, R. C. Flagan and J. H. Seinfeld, Ship impacts on the marine atmosphere: insights into the contribution of shipping emissions to the properties of marine aerosol and clouds, *Atmos. Chem. Phys.*, 2012, **12**, 8439–8458.

59 A. M. Aldhaif, D. H. Lopez, H. Dadashazar and A. Sorooshian, Sources, frequency, and chemical nature of dust events impacting the United States East Coast, *Atmos. Environ.*, 2020, **231**, 117456.

60 A. H. Mardi, H. Dadashazar, D. Painemal, T. Shingler, S. T. Seaman, M. A. Fenn, C. A. Hostetler and A. Sorooshian, Biomass Burning Over the United States East Coast and Western North Atlantic Ocean: Implications for Clouds and Air Quality, *J. Geophys. Res.:Atmos.*, 2021, **126**, e2021JD034916.

61 R. Bro and A. K. Smilde, Principal component analysis, *Anal. Methods*, 2014, **6**, 2812–2831.

62 A. F. Corral, Y. Choi, B. L. Collister, E. Crosbie, H. Dadashazar, J. P. Digangi, G. S. Diskin, M. Fenn, S. Kirschler, R. H. Moore, J. B. Nowak, M. A. Shook, C. T. Stahl, T. Shingler, K. L. Thornhill, C. Voigt, L. D. Ziemba and A. Sorooshian, Dimethylamine in cloud water: a case study over the northwest Atlantic Ocean, *Environ. Sci.: Atmos.*, 2022, **2**, 1534–1550.

63 C. Stahl, M. T. Cruz, P. A. Bañaga, G. Betito, R. A. Braun, M. A. Aghdam, M. O. Cambaliza, G. R. Lorenzo, A. B. MacDonald, M. R. A. Hilario, P. C. Pabroa, J. R. Yee, J. B. Simpas and A. Sorooshian, Sources and characteristics of size-resolved particulate organic acids and methanesulfonate in a coastal megacity: Manila, Philippines, *Atmos. Chem. Phys.*, 2020, **20**, 15907–15935.

64 T. S. Bates, B. K. Lamb, A. Guenther, J. Dignon and R. E. Stoiber, Sulfur emissions to the atmosphere from natural sourees, *J. Atmos. Chem.*, 1992, **14**, 315–337.

65 D. Davis, G. Chen, P. Kasibhatla, A. Jefferson, D. Tanner, F. Eisele, D. Lenschow, W. Neff and H. Berresheim, DMS oxidation in the Antarctic marine boundary layer: Comparison of model simulations and held observations of DMS, DMSO, DMSO2, H2SO4(g), MSA(g), and MSA(p), *J. Geophys. Res.:Atmos.*, 1998, **103**, 1657–1678.

66 C. Yang, S. Zhou, C. Zhang, M. Yu, F. Cao and Y. Zhang, Atmospheric Chemistry of Oxalate: Insight Into the Role of Relative Humidity and Aerosol Acidity From High-Resolution Observation, *J. Geophys. Res.:Atmos.*, 2022, **127**, e2021JD035364.

67 G. R. Lorenzo, L. D. Ziemba, A. F. Arellano, M. C. Barth, E. C. Crosbie, J. P. DiGangi, G. S. Diskin, R. Ferrare, M. R. A. Hilario, M. A. Shook, S. Tilmes, J. Wang, Q. Xiao, J. Zhang and A. Sorooshian, *Measurement Report: Characterization of Aerosol Hygroscopicity over Southeast Asia during the NASA CAMP2Ex Campaign*, EGUsphere, 2024, 2024, pp. 1–42.

68 M. R. A. Hilario, E. Crosbie, P. A. Bañaga, G. Betito, R. A. Braun, M. O. Cambaliza, A. F. Corral, M. T. Cruz, J. E. Dibb, G. R. Lorenzo, A. B. MacDonald, C. E. Robinson, M. A. Shook, J. B. Simpas, C. Stahl, E. Winstead, L. D. Ziemba and A. Sorooshian, Particulate Oxalate-To-Sulfate Ratio as an Aqueous Processing Marker: Similarity

Across Field Campaigns and Limitations, *Geophys. Res. Lett.*, 2021, **48**, e2021GL096520.

69 A. Sorooshian, E. Crosbie, L. C. Maudlin, J. S. Youn, Z. Wang, T. Shingler, A. M. Ortega, S. Hersey and R. K. Woods, Surface and airborne measurements of organosulfur and methanesulfonate over the western United States and coastal areas, *J. Geophys. Res.:Atmos.*, 2015, **120**, 8535–8548.

70 K. L. Hayden, A. M. Macdonald, W. Gong, D. Toom-Sauntry, K. G. Anlauf, A. Leithead, S.-M. Li, W. R. Leaitch and K. Noone, Cloud processing of nitrate, *J. Geophys. Res.:Atmos.*, 2008, **113**, D18201.

71 H. Xue and G. Feingold, A modeling study of the effect of nitric acid on cloud properties, *J. Geophys. Res.:Atmos.*, 2004, **109**, D18204.

72 K. Kawamura and S. Bikkina, A review of dicarboxylic acids and related compounds in atmospheric aerosols: Molecular distributions, sources and transformation, *Atmos. Res.*, 2016, **170**, 140–160.

73 A. Sorooshian, V. Varutbangkul, F. J. Brechtel, B. Ervens, G. Feingold, R. Bahreini, S. M. Murphy, J. S. Holloway, E. L. Atlas, G. Buzorius, H. Jonsson, R. C. Flagan and J. H. Seinfeld, Oxalic acid in clear and cloudy atmospheres: Analysis of data from International Consortium for Atmospheric Research on Transport and Transformation 2004, *J. Geophys. Res.:Atmos.*, 2006, **111**, D23S45.

74 B. Ervens, A. Sorooshian, A. M. Aldhaif, T. Shingler, E. Crosbie, L. Ziemba, P. Campuzano-Jost, J. L. Jimenez and A. Wisthaler, Is there an aerosol signature of chemical cloud processing?, *Atmos. Chem. Phys.*, 2018, **18**, 16099–16119.

75 J. Z. Yu, X. F. Huang, J. Xu and M. Hu, When aerosol sulfate goes up, so does oxalate: implication for the formation mechanisms of oxalate, *Environ. Sci. Technol.*, 2005, **39**, 128–133.

76 L. C. Maudlin, Z. Wang, H. H. Jonsson and A. Sorooshian, Impact of wildfires on size-resolved aerosol composition at a coastal California site, *Atmos. Environ.*, 2015, **119**, 59–68.

77 R. A. Braun, H. Dadashazar, A. B. MacDonald, A. M. Aldhaif, L. C. Maudlin, E. Crosbie, M. A. Aghdam, A. Hossein Mardi and A. Sorooshian, Impact of Wildfire Emissions on Chloride and Bromide Depletion in Marine Aerosol Particles, *Environ. Sci. Technol.*, 2017, **51**, 9013–9021.